Existence and stability of skyrmion bags in thin magnetic films

Charles Kind,[1,*] Sven Friedemann,[2] and Dan Read[3]

[1] *School of Mathematics, University of Bristol, Bristol BS8 1TW, UK*
[2] *HH Wills Physics Laboratory, University of Bristol, Bristol BS8 1TL, UK*
[3] *School of Physics and Astronomy, Cardiff University, Cardiff CF24 3AA, UK*

(Dated: November 29, 2019)

Skyrmion bags are spin textures of any integer topological degree, realised in micromagnetic simulations and experimentally in liquid crystals. They have been proposed as a promising new form of magnetic data storage due to their stability with respect to perturbations and the possibility of encoding different values in topologically distinct magnetisation configurations. We simulate skyrmion bags in magnetic thin films having a range of physically realistic material parameters. The results give a range over which stable skyrmion bags may be found in experiment and we extract a relationship to help guide production of these potentially useful quasiparticles.

Individual magnetic skyrmions are stable, particle-like, spin configurations in the magnetisation of chiral magnets [1]. Their stability is derived from the skyrmion's topological nature. A single skyrmion in the continuous model is a perfect cover of the two-sphere, illustrated in figure 1**c**, and hence impossible to unwind. This stability, coupled with the low currents required to move them, makes them seem attractive as candidates for future forms of magnetic data storage with read-write capabilities [2].

Skyrmions have been observed with radii of the order of nanometres and due to the relative weakness of inter-skyrmion reactions can be densely packed. A single skyrmion can however only represent a binary bit, in current racetrack models [3], where change in the distance between skyrmions could lead to data loss. Hence the interest in higher topological degree skyrmions which could encode more data per texture and yet retain the benefits of unitary degree skyrmions [4][5].

Skyrmion bags [4], or sacks [5], are nested skyrmionic structures of any integer topological degree. Typically composed of a single skyrmion outer boundary and then a number of inner antiskyrmions which can themselves contain skyrmions. This pattern may continue with skyrmions or antiskyrmions contained within their opposing degree partners. In two dimensional (2D) models describing thin films bags can be described by the total topological degree defined as

$$Q = \frac{1}{4\pi} \int \boldsymbol{n} \cdot (\partial_x \boldsymbol{n} \times \partial_y \boldsymbol{n})\, dxdy, \tag{1}$$

where $\boldsymbol{n}(\boldsymbol{x})$ is the unit vector field of the magnetisation. With this definition a single skyrmion has the degree $Q = -1$.

Skyrmion bags, being composed of any number of skyrmions and antiskyrmions, could give rise to an infinite variety of bag configurations at any degree. We use a notation to define the degree of each grouping of (anti)skyrmions within the bag. An $S(n)$ bag is one with n antiskyrmions and a total degree of $Q = n - 1$. As an antiskyrmion's degree has an opposite sign to a skyrmion, structures like the $S(1)$ bag, shown in 1**d**, also know as skyrmionium or target skyrmions [6][7], have a total degree of zero.

Skyrmions and, as we show here, skyrmion bags occur in magnetic materials with inversion asymmetry. In materials with uniaxial anisotropy, which we consider here, they can have either a Néel or Bloch type, shown in figures 1**a,b** respectively, determined by the dominant type of Dzyaloshinskii-Moriya interaction (DMI) present. In thin film multilayers the DMI results in Néel type skyrmions which, when projected onto the two sphere, have vectors normal to the surface and have been called hedgehog skyrmions [8]. In this paper we look exclusively at Néel type skyrmions but the technique illustrated here could also be applied in Bloch type configurations.

In thin films hosting skyrmions the magnetic characteristics can be tuned through changes to composition and thicknesses of individual layers. The magnetic properties of the ferromagnetic material sandwiched between heavy metal layers can be altered[9]. DMI interactions, which are caused by spin orbit coupling (SOC), can be tuned[10]. The thickness of the magnetic layer can also affect DMI and the demagnetising field. More subtle variation of the DMI in thin films produced via magnetron sputtering have also been reported by varying the thickness of an adjacent oxide layer [11] or by modifying the deposition conditions such as sputter chamber base pressure [12]. Magnetocrystalline anisotropy, which also derives from SOC, can also be altered in these multilayers[13].

In this letter, using micromagnetic simulations, we analyse skyrmion bags for a range of physical constants that are relevant to known experimentally realised magnetic multilayers such as CoPt, see table I. With a range of permissible magnetic parameters, we show where we may find skyrmion bags.

* charles.kind@bristol.ac.uk

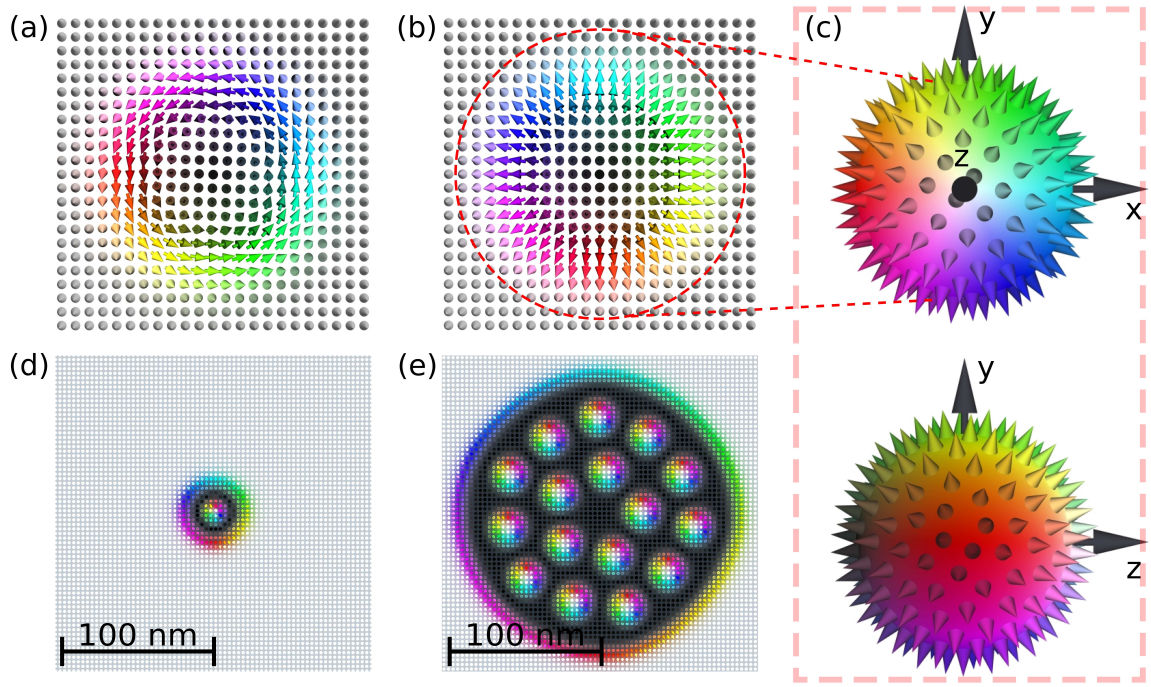

Figure 1: **Skyrmion and skyrmion bag configurations.** **(a)** A Bloch skyrmion. **(b)** A Néel skyrmion. **(c)** The Runge colour sphere with spins pointing normal to the surface. The top sphere representing the mapping of the Neèl skyrmion **(b)** to S^2, assuming that the marked path contains only unit vectors in the $+e_z$ direction. **(d)** A stable Mumax3 simulated $S(1)$ bag for constants $A_{ex} = 10$ pJm^{-1}, $D_{\text{DMI}} = 2.5$ mJm^{-2} and $K_{\text{u}} = 0.7$ MJm^{-3} on a 1024×1024 nm^2 square of 1 nm thickness with a fixed boundary. **(e)** A stable Mumax3 simulated $S(16)$ bag for the same constants and domain as in **(d)**.

Table I: Magnetic parameters for materials hosting skyrmions.

Exchange A_{ex} pJm^{-1}	**DMI** D_{DMI} mJm^{-2}	**Anisotropy** K_{u} MJm^{-3}	**Material**	**Ref**
8	0.1	2	FePt	[14]
14	1.68	0.779	Pt/CoFeB/MgO	[15]
15	3	0.8	CoPt	[14]
20	4	0.8	CoFeB	[16]

The simulations where performed using the GPU-accelerated micromagnetic simulation program MuMax3 [17] with Landau-Lifshitz dynamics in the form

$$\frac{\partial \boldsymbol{n}}{\partial t} = \gamma \frac{1}{1+\alpha^2} \left(\boldsymbol{n} \times \boldsymbol{B}_{\text{eff}} + \alpha \boldsymbol{n} \times (\boldsymbol{n} \times \boldsymbol{B}_{\text{eff}}) \right), \qquad (2)$$

where $\gamma \approx 176$ rad(ns T)$^{-1}$ is the electron gyromagnetic ratio, $\alpha = 0.3$ the dimensionless damping parameter, $\boldsymbol{B}_{\text{eff}} = \delta E / \delta \boldsymbol{n}$ the effective magnetic field and $\boldsymbol{n}(\boldsymbol{x}) = \boldsymbol{N}(\boldsymbol{x})/M_s$ the magnetisation vector field normalised by the saturation magnetisation. The initial bag configurations were built from template functions of individual skyrmions and antiskyrmions, in the $S(1)$ and $S(16)$ configurations. The simulations showed a significant drop in energy from the initial condition which indicates the system achieving stability. These bags where chosen to represent experimentally realised skyrmionium, $S(1)$, and, to explore the potential for skyrmion bags with a large range of data encoding, the $S(16)$, which is expected to be more stable than the $S(1)$ [4]. Sixteen distinct configurations allow for the encoding of 4 bits of data.

The micromagnetic energy functional is evaluated as

$$E(\boldsymbol{n}) = E_{\text{ex}} + E_{\text{DMI}} + E_{\text{demag}} + E_{\text{anis}} \qquad (3)$$

where,

$$E_{\text{ex}} = A_{\text{ex}} \int (\nabla \boldsymbol{n})^2 \, dxdy \qquad (4)$$

$$E_{\text{DMI}} = D_{\text{DMI}} \int [n_z (\nabla \cdot \boldsymbol{n}) - (\boldsymbol{n} \cdot \nabla) n_z] \, dxdy \qquad (5)$$

$$E_{\text{demag}} = \mu_0 M_s / 2 \int (\boldsymbol{H}_{\text{demag}} \cdot \boldsymbol{n}) \, dxdy \qquad (6)$$

$$E_{\text{anis}} = K_{\text{u}} \int (1 - (n_z)^2) \, dxdy, \; K_{\text{u}} > 0. \qquad (7)$$

These being the Heisenberg exchange, antisymmetric exchange (DMI), demagnetisation, and easy axis anisotropy energies respectively. $\boldsymbol{H}_{\text{demag}}$, in equation 6 is the demagnetising field which is calculated from the magnetisation at each time step [17].

The simulation geometry is a 1024×1024 nm^2 square of 1 nm thickness, in order to represent a typical wire that could be fabricated using lithographic processing. Cell size of $2 \times 2 \times 1$ nm^3 has been used. Uniform material parameters are: saturation magnetisation $M_s = 580$

kAm^{-1} [14] and the uniaxial anisotropy is along the $+z$ direction, normal to the film. Exchange is selected from $\{10, 15, 20\}$ pJm^{-1}, interfacial DMI is in the range $[2, 4.3]$ mJm^{-2} in steps of 0.1 mJm^{-2} and uniaxial anisotropy $[0.6, 0.8]$ MJm^{-3} in steps of 0.05 MJm^{-3} to cover the range of possible materials parameters (table I).

The simulations used Mumax3's periodic boundary conditions and were run to simulate 100 ns with the vector field analysed every one ns to test if the magnetisation remains stable over time and to calculate the topological degree (1). At each grouping of constants we test $S(1)$ and $S(16)$ bags (Fig. 1**d,e**) for stability. A structure was considered stable if the measured total energy varied by less than one part in 10^5 for at least 10 ns. Typically, stable structures would achieve equilibrium within 20 ns of the start of the simulation.

In order to guide our search for micromagnetic regimes where skyrmion bags could be stable, we seek a family of parameters $A_{ex}, D_{\text{DMI}}, K_{\text{u}}$ that have comparable minimum energy magnetisation configurations $\boldsymbol{n}(\boldsymbol{x})$. A Derrick scaling argument [18] on the energy functional (3) provides us with an expected stability condition. Perturbing the magnetisation by rescaling space defining $\boldsymbol{n}_\lambda(x) = \boldsymbol{n}(\lambda x)$, where λ is an arbitrary constant gives,

$$E_\lambda = A_{ex} I_1 + D_{\text{DMI}} I_2/\lambda + K_{\text{u}} I_3/\lambda^2. \tag{8}$$

Where,

$$I_1 = \int (\nabla \boldsymbol{n})^2 \, dxdy \tag{9}$$

$$I_2 = \int [n_z (\nabla \cdot \boldsymbol{n}) - (\boldsymbol{n} \cdot \nabla) n_z] dxdy \tag{10}$$

$$I_3 = \int (1 - (n_z)^2) dxdy \text{ for } (x, y) \in \mathbb{R}^2. \tag{11}$$

If $(dE_\lambda/d\lambda)|_{\lambda=1} = -D_{\text{DMI}} I_2 - 2K_{\text{u}} I_3 = 0$ then stable skyrmions exist and,

$$K_{\text{u}} = -D_{\text{DMI}} I_2/2I_3 = m \cdot D_{\text{DMI}}. \tag{12}$$

This is a type of virial constraint [19]. Therefore we expect to find the same magnetisation configurations at critical points of the energy functional as we follow the integral curve (12) varying the coefficients of anisotropy and DMI. We note that this equation is in the form of a straight line with slope m through the origin. In the Derrick scaling we exclude the demagnetisation term as is often done in micromagnetic energy functional analysis [5]. However by analysing the stability range obtained in our simulations with a straight line as suggested by equation (12) we include the demagnetisation as an effective anisotropy [20][21]. Indeed we find good correspondence of our results to equation (12).

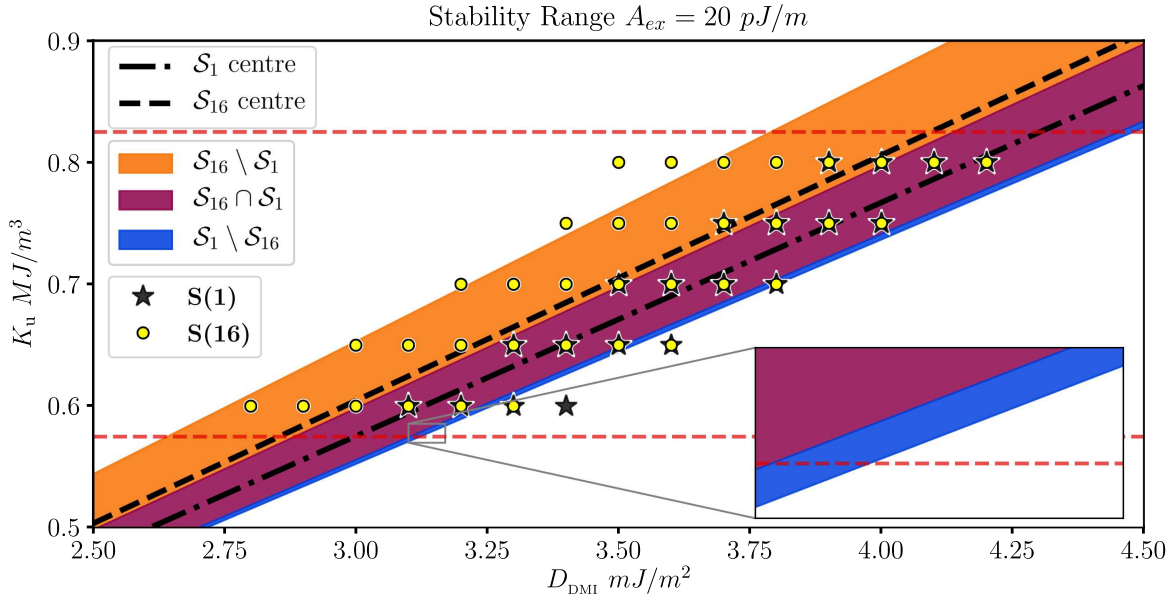

Figure 2: **Stability ranges for $S(1)$ and $S(16)$ bags.** Plot for $A_{ex} = 20$ pJm^{-1}. We define the set $\mathcal{S}_n = \{(D_{\text{DMI}}, K_u, A_{ex}) \in \mathbb{R}^3 \mid \text{Skyrmion bag of type } S(n) \text{ is stable}\}$, in this plot we approximate these sets by fixing the exchange constant A_{ex} and shading the areas corresponding to gradients within one σ of the critical gradient taken from table (II). The horizontal dashed lines represent the boundary of the simulations we have performed. The inset highlights that $\mathcal{S}_1 \setminus \mathcal{S}_{16}$ is not empty for this approximation.

In Fig. 2 we show the range of K_u and D_{DMI} for $A_{ex} = 20\ \mathrm{pJm^{-1}}$. Stable $S(1)$ and $S(16)$ bags are found roughly along a straight line through the origin as expected based upon our Derrick scaling analysis. We tabulate the slopes of the centre lines of $S(1)$ and $S(16)$ bags for all simulated A_{ex} in table (II). We find the central gradient line for a bag type, $S(1)$ or $S(16)$, at a particular exchange energy, by finding the gradient at each data point, summing over all relevant points and dividing by the total number. We assume the gradients are normally distributed, supported by Q-Q plots and Anderson Darling [22] and record the results.

Our results indicate that the $|2\sigma|$ range of $S(1)$ is entirely encompassed by the $|2\sigma|$ range for the $S(16)$ bags, at all exchange constants tested, therefore the ideal parameter range to find bags lies within the $|1\sigma|$ range for $S(1)$ (see Fig. 2).

Table II: Critical line gradients (2 s.f.).

Exchange A_{ex} $\mathrm{pJm^{-1}}$	**Type**	**Gradient** m $\mathrm{pm^{-1}}$	**Standard Deviation** σ $\mathrm{pm^{-1}}$
10	$S(1)$	2.72	0.08
10	$S(16)$	2.84	0.14
15	$S(1)$	2.22	0.08
15	$S(16)$	2.32	0.14
20	$S(1)$	1.92	0.08
20	$S(16)$	2.01	0.16

For applications, a stable size of skyrmion bag will be important. We analyse bag diameters as we vary DMI and anisotropy. We find that there are bags, at each set of constants, varying in size by less than 5% from their average width. We analyse the polar angle profiles of the $S(1)$ bags, as shown in Fig. 3, for a range of DMI at $A_{ex} = 20\ \mathrm{pJm^{-1}}$ and $K_{\mathrm{u}} = 0.7$, by taking the midline, $y = 0$, of the simulated area and extracting the angle at every cell Fig.3**b**. The outer edge of a bag, in this study, is considered the first cell on the midline, from the left or right hand domain sides, where the polar angle was greater than 150°.

Table III: Fitted straight lines at $A_{ex} = 20\ \mathrm{pJm^{-1}}$ for $S(1)$ (2 s.f.). Fitted values of the anisotropy K_{u}^{fit} at a given DMI where calculated with eq. 12 using the value for m in Table II.

Anisotropy K_{u} $\mathrm{MJm^{-3}}$	**DMI** D_{DMI} $\mathrm{mJm^{-2}}$	**Diameter** nm	**Fitted** K_{u}^{fit} $\mathrm{MJm^{-3}}$	**Difference** $\Delta K_{\mathrm{u}}/K_{\mathrm{u}}^{fit}$ %
0.6	3.1	74	0.62	3.5
0.65	3.3	70	0.66	1.75
0.7	3.5	70	0.7	0.2
0.75	3.7	70	0.74	-1.13
0.8	3.9	70	0.78	-2.3

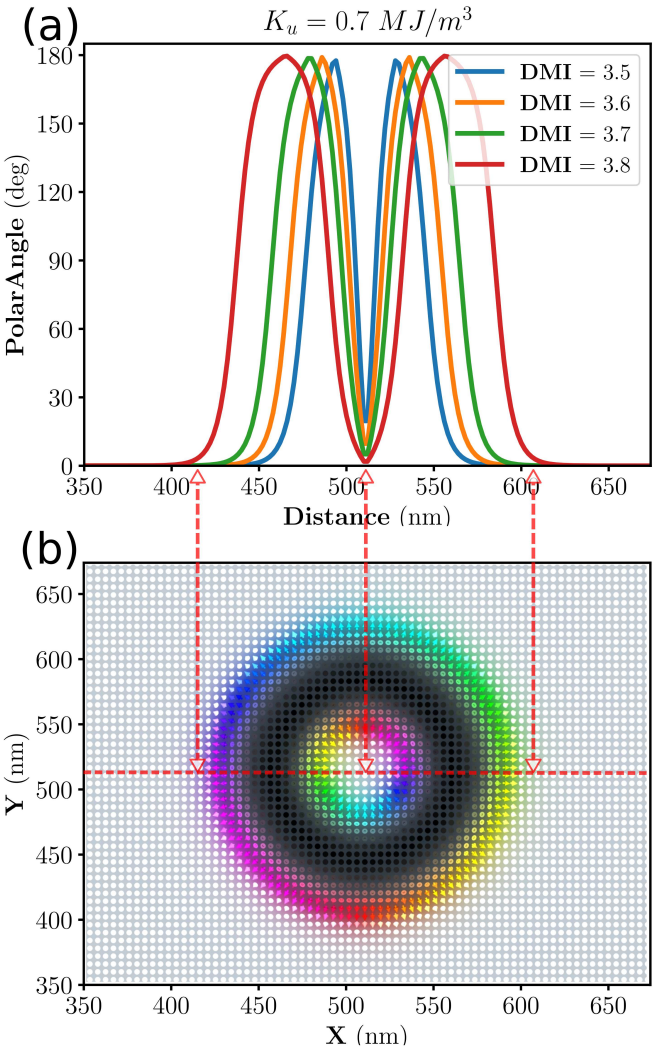

Figure 3: **Polar angle of magnetisation profiles of $S(1)$ bags for DMI at $A_{ex} = 20\ \mathbf{pJm^{-1}}$ and $K_{\mathrm{u}} = 0.7$. (a)** Polar profiles. **(b)** A stable Neèl type skyrmion for $D_{\mathrm{DMI}} = 3.8\ \mathrm{mJm^{-2}}$ and $K_{\mathrm{u}} = 0.7\ \mathrm{MJm^{-3}}$ with arrowed lines mapping from the center line of the skyrmion to the appropriate points on the profile **(b)**.

Table III shows that skyrmion bags of similar size can indeed be found as we vary the critical constants of Anisotropy and DMI. We also note that for a fixed exchange energy and anisotropy, increasing DMI within the stable regime increases bag size super-linearly as can be seen from the profile widths Fig. 3**a** . Hence for tightness of spin textures, which is important for higher areal density data storage, the lower end of the stable DMI range is to be preferred.

In summary, we have found a range of constants, associated with a linear function and a variation, where we have high confidence that skyrmion bags will be stable. Our analysis shows linear center lines $K_{\mathrm{u}} = m \cdot D_{\mathrm{DMI}}$ around which stable $S(1)$ and $S(16)$ bags are found respectively (see Tab. II). This linear form agrees with the expected form of a Derrick scaling analysis and high-

lights that corrections from demagnetisation act as effective anisotropy.

From the results obtained we expect that along the $S(1)$, skyrmionium, centre line, at any given exchange energy, is the ideal starting point for the seeding and observation of skyrmion bags in thin film multilayers.

Equation (12) should be an effective tool to aid in the experimental realisation of skyrmion bags in magnetic multilayers. The existence of suitable experimental methods to vary these parameters should allow fine tuning of appropriate samples.

ACKNOWLEDGEMENTS

Dan Read gratefully acknowledges support from the Leverhulme Trust via an International Academic Fellowship (IAF-2018-039). This work was supported in part by the UK Engineering and Physical Sciences Research Council (EPSRC) grant EP/M506473/1. The Titan V GPU used for parts of this research was donated by the NVIDIA Corporation.

[1] A. Bogdanov and A. Hubert. *Journal of Magnetism and Magnetic Materials*, 138(3):255–269, December 1994.

[2] Albert Fert, Vincent Cros, and João Sampaio. *Nature Nanotechnology*, 8(3):152–156, March 2013.

[3] Albert Fert, Nicolas Reyren, and Vincent Cros. *Nature Reviews Materials*, 2(7):17031, July 2017.

[4] David Foster, Charles Kind, Paul J. Ackerman, Jung-Shen B. Tai, Mark R. Dennis, and Ivan I. Smalyukh. *Nature Physics*, April 2019.

[5] Filipp N. Rybakov and Nikolai S. Kiselev. *Physical Review B*, 99(6):064437, February 2019.

[6] M. Finazzi, M. Savoini, A. R. Khorsand, A. Tsukamoto, A. Itoh, L. Duò, A. Kirilyuk, Th. Rasing, and M. Ezawa. *Physical Review Letters*, 110(17):177205, April 2013.

[7] Xichao Zhang, Jing Xia, Yan Zhou, Daowei Wang, Xiaoxi Liu, Weisheng Zhao, and Motohiko Ezawa. *Physical Review B*, 94(9):094420, September 2016.

[8] Wanjun Jiang, Wei Zhang, Guoqiang Yu, M. Benjamin Jungfleisch, Pramey Upadhyaya, Hamoud Somaily, John E. Pearson, Yaroslav Tserkovnyak, Kang L. Wang, Olle Heinonen, Suzanne G. E. te Velthuis, and Axel Hoffmann. *AIP Advances*, 6(5):055602, March 2016.

[9] Frances Hellman, Axel Hoffmann, Yaroslav Tserkovnyak, Geoffrey S. D. Beach, Eric E. Fullerton, Chris Leighton, Allan H. MacDonald, Daniel C. Ralph, Dario A. Arena, Hermann A. Dürr et al. *Reviews of Modern Physics*, 89(2):025006, June 2017.

[10] Hongxin Yang, Olivier Boulle, Vincent Cros, Albert Fert, and Mairbek Chshiev. *Scientific Reports*, 8(1):12356, August 2018.

[11] Anni Cao, Xueying Zhang, Bert Koopmans, Shouzhong Peng, Yu Zhang, Zilu Wang, Shaohua Yan, Hongxin Yang, and Weisheng Zhao. *Nanoscale*, 10(25):12062–12067, July 2018.

[12] Adam W. J. Wells, Philippa M. Shepley, Christopher H. Marrows, and Thomas A. Moore. *Physical Review B*, 95(5):054428, February 2017.

[13] Jun Hu, Peng Wang, Jijun Zhao, and Ruqian Wu. *Advances in Physics: X*, 3(1):1432415, January 2018.

[14] J. Sampaio, V. Cros, S. Rohart, A. Thiaville, and A. Fert. *Nature Nanotechnology*, 8(11):839–844, November 2013.

[15] Seonghoon Woo, Kyung Mee Song, Hee-Sung Han, Min-Seung Jung, Mi-Young Im, Ki-Suk Lee, Kun Soo Song, Peter Fischer, Jung-Il Hong, Jun Woo Choi, Byoung-Chul Min, Hyun Cheol Koo, and Joonyeon Chang. *Nature Communications*, 8:ncomms15573, May 2017.

[16] R. Tomasello, E. Martinez, R. Zivieri, L. Torres, M. Carpentieri, and G. Finocchio. *Scientific Reports*, 4:6784, October 2014.

[17] Arne Vansteenkiste, Jonathan Leliaert, Mykola Dvornik, Mathias Helsen, Felipe Garcia-Sanchez, and Bartel Van Waeyenberge. *AIP Advances*, 4(10):107133, October 2014.

[18] G. H. Derrick. *Journal of Mathematical Physics*, 5(9):1252–1254, September 1964.

[19] R. Clausius. *The London, Edinburgh, and Dublin Philosophical Magazine and Journal of Science*, 40(265):122–127, August 1870.

[20] Robert C. O'Handley. Wiley, January 2000.

[21] A. Bogdanov and A. Hubert. *Journal of Magnetism and Magnetic Materials*, 195(1):182–192, April 1999.

[22] T. W. Anderson and D. A. Darling. *The Annals of Mathematical Statistics*, 23(2):193–212, 1952.